metals

MDPI

Article

3D Printing Using Ti-Al Nanopowders: Mechanisms of Structure Formation

Vladimir Promakhov [1,*], Alexey Matveev [1], Artem Babaev [1], Nikita Schulz [1], Nikita Toropkov [1,2], Alexander Vorozhtsov [1] and Marat Lerner [1,2]

[1] Scientific and Educational Center "Additive Technologies", National Research Tomsk State University, 634050 Tomsk, Russia;
[2] Laboratory of Physical Chemistry of Highly Dispersed Materials, Institute of Strength Physics and Materials Science Siberian Branch of Russian Academy of Sciences, 634055 Tomsk, Russia
* Correspondence: vvpromakhov@mail.ru

Abstract: In the presented research work, 3D materials were fabricated by additive moulding by means of extrusion of a mixture of high filled polymers and nanopowders of Ti-Al intermetallides with subsequent sintering at 1100 ± 20 °C, 1200 ± 20 °C and 1250 ± 20 °C (MEAM-HP process). Nanopowders of Ti-Al intermetallides were obtained by the electrical explosion of intertwined aluminium and titanium wires. It was found that the structure of the materials comprises an AlTi matrix with Ti_2AlN MAX-phase particles distributed within it, surrounded by a composite layer of Ti_3Al-Ti_2AlN. Sintering temperature increases led to changes in the concentration of TiAl, Ti_3Al and Ti_2AlN phases in the samples. Besides that, aluminium oxide particles were discovered in the structure of the materials. It was found that as the sintering temperature was increased from 1100 ± 20 °C to 1250 ± 20 °C, the average microhardness of the samples increased from 193 to 690 $HV_{0.1}$.

Keywords: nanopowders; additive technology; structure; phase composition

Citation: Promakhov, V.; Matveev, A.; Babaev, A.; Schulz, N.; Toropkov, N.; Vorozhtsov, A.; Lerner, M. 3D Printing Using Ti-Al Nanopowders: Mechanisms of Structure Formation. *Metals* **2022**, *12*, 1737. https://doi.org/10.3390/met12101737

Academic Editors: Victor A. Klinkov, Vera Popovich and Matteo Benedetti

Received: 02 August 2022
Accepted: 12 October 2022
Published: 16 October 2022

1. Introduction

The main requirement put forward for materials by aerospace and transportation industries is minimal density while retaining required mechanical properties [1]. The density of intermetallides based on titanium and aluminium is as follows: Al-Ti (titanium aluminide) has density that is 1.5–3 times lower than that of alloys based on nickel and titanium, and their mechanical properties (tensile strength, yield stress, etc.) at room temperature and increased temperature are comparable or superior to those of the alloys [2,3]. Additionally, intermetallides of this grade have higher resistance to oxidation and corrosion, which allows for their use in aggressive media at increased temperatures [4–7]. Titanium aluminides are successfully used in the fabrication of turbine blades for aircraft engines, as well as for wheel disks and exhaust valves of automotive engines [8–11]. With these materials, part weight can be reduced to 55% of that of nickel alloys, thus increasing fuel efficiency while lowering carbon footprint, which is in line with the trends in the development of state-of-the-art, environmentally conscious manufacturing technologies [12,13]. Materials based on Ti-Al intermetallides are normally manufactured by sintering micron-size powders of aluminium and titanium [14]. However, in this case, sintered materials undergo considerable expansion caused by the emergence of the $TiAl_3$ phase at early sintering stages [15]. Additionally, great differences in the diffusion coefficients of titanium and aluminium leads to the manifestation of the Kirkendall effect [16], which is associated with the emergence of large pores and cracks in the volume of materials in the course of sintering [17]. Hot pressing and plasma spark sintering are the most popular approaches to the fabrication of dense materials from Al-Ti intermetallides, as they prevent emergence of pores and cracks in the fabricated items [18–20]. Thus, in [21], the

authors demonstrated successful use of a plasma sintering process to obtain dense materials from Ti-Al powder mixture with the concentration of titanium at 20, 50 and 80 vol %. Sintering was carried out at 600 °C and 200 MPa over 5 min in air. In [21], it was shown that plasma spark sintering produced intermetallide composites such as Al-Ti with isle structure that comprised Al_3Ti, Al_5Ti_2 and $Al_{11}Ti_5$ phases distributed within the aluminium or titanium matrix (depending on the composition of the initial mixture). The research authors found that there were no pores in the materials obtained while their density was close to the theoretically estimated one. The Vickers hardness of high strengthened areas in the materials obtained from the powder mixtures with titanium concentration of 20, 50 and 80 vol % was 75, 300 and 363 HV, respectively. Despite high efficiency of spark plasma sintering, use of other Ti-Al intermetallide fabrication processes that would be more efficient and economically viable remains an open issue. As of now, additive manufacturing technologies [22] are one of the most promising processes for fabricating materials based on this composition. Additive manufacturing (AM) technologies reached maturity around the year 2010 [23]. Use of AM allows for fabricating items with complex geometry while reducing required human resources, financial costs and production waste products [24]. Khorasani M. et al. [25] demonstrated calculations of laser growth parameters affecting the production cost of a jet engine air collector. These parameters include a powder layer laser cladding process, machining, raw materials, labour costs and post-processing. The parameters were compared to determine the best production strategy. The results of the work showed that AM can solve a number of problems and can improve production through customisation, rapid prototyping and geometric freedom. The authors found that 49–58% of the cost is associated with pre- and post-processing when using laser technology to produce an air collector. Thus, in [26], materials based on the Al-Ti intermetallide were manufactured by direct laser deposition. According to the research findings, the structure of the obtained materials was comprised of platelike γ-TiAl and α_2-Ti_3Al grains, their size varying from 50 to 100 μm. An investigation into the mechanical properties revealed that Vickers hardness of the materials was 425 HV, and tensile strength was 650 MPa. Here the authors state that the nature of sample destruction was intercrystallite. Chen W. et al. showed in [27] that the replacement of high-temperature, nickel-based alloys with materials additive manufactured from Al-Ti intermetallide has made it possible to reduce engine weight by 100 kg while increasing fuel efficiency by 20%.

Important drawbacks of Al-Ti intermetallides are their low plasticity and impact strength at room temperature, as well as their low creep strength at high temperatures (700–750 °C) [28]. Li X. et al. showed, in [29], that improved mechanical properties are achieved by obtaining fine-grain structure of materials by sintering nanosize particles of the Al-Ti intermetallide. Additionally, the use of nanosize powders will allow the emergence of Kirkendall pores to be suppressed during materials sintering.

Successful use of electro-explosive synthesis to produce nanosize Al-Ti intermetallide powders from intertwined aluminium and titanium wires (with the diameter of 0.35 mm and 0.32 mm, respectively) was demonstrated in [30]. In this work, it was shown that electro-explosive synthesis produces micronsize and nanosize particles of an Al-Ti intermetallide. Increasing voltage input into the wires from 22 kV to 29 kV leads to the production of a reduced share of micron-size particles and average powder particle size reduction from 240 to 133 nm. XRD analysis results have shown the presence of γ-TiAl phases (68.3–78.0 wt%), α2-Ti3Al (7.8–9.2 wt%), α-Ti (14.2–22.3 wt%). Next, 10.05 ± 0.05 mm thick tablets were pressed from the powders obtained; the tablets were then sintered in a vacuum furnace in the temperature range of 800–1250 °C. The authors have determined that in the course of sintering at 1250 °C, fully sintered samples are produced with platelike structure [31] and relative density of 92%. It was shown in the research that diffusion of aluminium towards titanium is taking place in the process of sintering, which leads to the emergence of Ti2Al, TiAl2 and TiAl3 phases. From the data obtained, we can conclude that the process of electro-explosion of intertwined wires made of aluminium and titanium can be used to obtain Al-Ti powder, and that this is a promising technique

for the fabrication of 3D materials. However, the use of nanosize powders in the direct laser deposition process is impossible, as they do not have sufficient fluidity, and this may lead to nozzle clogging and deposition process disruption.

The solution to this problem lies in additive manufacturing of materials via extrusion of high-filled polymers that consist of a polymer binder and a powder filler. This technology is a multi-stage process whereby the polymer material is used as a binder for shaping the item during additive deposition. Then, the binder is removed by chemical, thermal or thermochemical treatment, and the fabricated workpiece is subjected to conventional sintering in a vacuum furnace [32]. In [33], Seyedzavvar M. and Boğa C. demonstrated the successful use of an acrylonitrile–butadiene–styrene binder filled with $CaCO_3$ nanoparticles as a feedstock for obtaining samples by the method of extrusion additive technologies. The addition of nanoparticles led to a significant increase in the tensile strength of the obtained samples. The authors of the work showed that the increase in strength is achieved due to the creation of uniformly distributed microvoids due to the blunting effect of $CaCO_3$ nanoparticles in the polymer matrix. Despite the fact that the authors of the work did not set the task of removing the polymer binder, they managed to obtain bulk samples with a uniform structure.

The purpose of the present research is investigating the formation of the structure of materials based on Ti-Al intermetallides obtained via additive manufacturing. A distinctive novelty of the approaches used herein lies in the use of nanopowders that allow the sintering temperature to be lowered and a unique material structure to be obtained.

2. Materials and Methods

To fabricate 3D materials by additive manufacturing via extrusion, a mixture of Al-Ti intermetallide powders and a polymer binder were prepared. Powders of nanosize intermetallides were produced by electro-explosive synthesis. The production technique was presented in [30]. Aluminium (Ø = 0.35 mm) and titanium (Ø = 0.32 mm) wires were intertwined and placed in an air-tight unit block that was then vacuumized and filled with argon to reach the pressure of 0.2 MPa. The synthesis process was initialised by energising the wires at 25 kV from a high-voltage power source. The average intermetallide powder particle size was 180 nm. Intermetallide powders obtained were mixed with the MC2162 polymer binder (Emery Oleochemicals, Loxstedt, Germany) at a ratio of 60:40 vol%. The MC2162 binder is a mixture of polyol ether and polyamide. The mixing was carried out in an argon-filled glove box with an SPQ-10 Z-blade mixer (Welber, Hangzhou, China) at a rotational speed of 60 rpm over 6 h. Then the mixture obtained was placed into an LE45-30 single-screw extruder and heated to 145 °C to produce feedstock. After that, rectangular block samples with the dimensions 10 mm × 10 mm × 5 mm (L × W × H) were fabricated by additive manufacturing by extrusion. A schematic layout of the laboratory unit for additive manufacturing of samples by extrusion is presented in Figure 1.

To remove the binder, chemical treatment of sample in acetone was performed. The samples obtained were heated in the vacuum furnace to 600 °C for 1 h and further subjected to high-temperature sintering at 1100 °C, 1200 °C and 1250 °C for at least 1 h.

The phase composition of the produced samples was studied on a Shimadzu XRD-6000 diffractometer (Shimadzu Corporation, Kyoto, Japan) on CuKα radiation. Crystal lattices from the Powder Diffraction File 4 database were used for reference. The phase composition, lattice parameters and bcc size were calculated by the refinement of the structure via full-profile analysis (Rietveld method). The structure of the samples was observed on a Tescan MIRA 3 LMU scanning electron microscope (TESCAN ORSAY HOLDING, Brno, Czech Republic) fitted with an Oxford Instruments Ultim Max 40 energy-dispersive detector (Oxford Instruments, High Wycombe, UK). Sample microhardness was measured on a Buehler Wilson Micromet 6040 hardness meter (Buehler LLC, Lake Bluff, Illinois, USA).

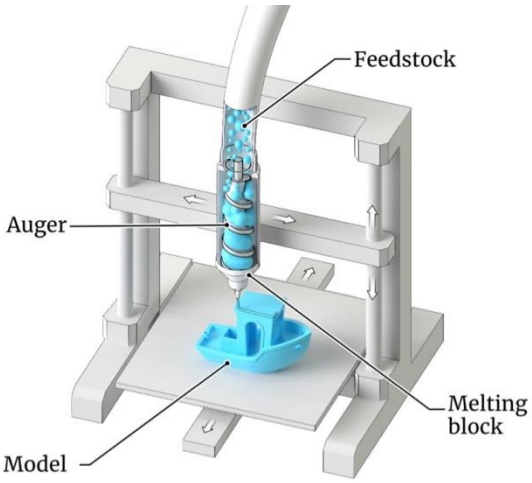

Figure 1. Schematic layout of the laboratory unit for additive manufacturing of samples by extrusion.

For example, Figure 2 shows the samples obtained from nanostructured powders based on Ti-Al. Figure 2a shows the sample after 3D printing and removal of the binder. Figure 2b shows a sample after 3D printing and high-temperature sintering. The study of the features of sintering samples in a vacuum furnace showed that the shrinkage is 23.4%. This shrinkage is justified by the use of nanopowders. It was found that thermal cracks and cracks between the layers of the material were not observed in the structure of the material.

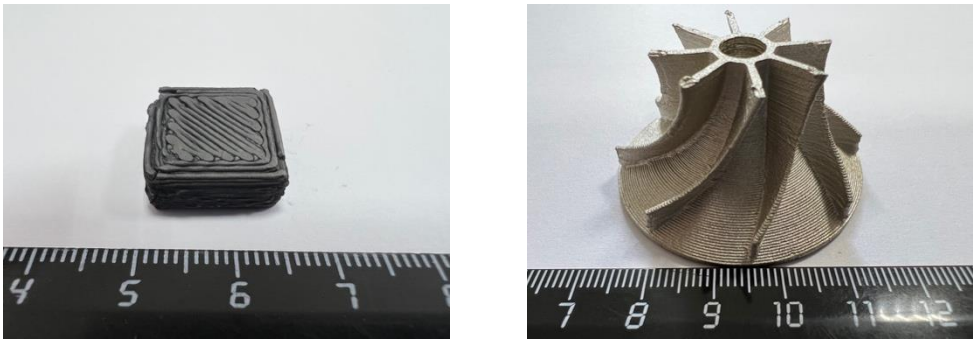

(**a**) (**b**)

Figure 2. Samples based on nanopowders Ti-Al obtained using additive technologies: (**a**) Experimental samples based on Ti-Al intermetallic nanopowders (green detail); (**b**) demonstration sample based on Ti-Al intermetallic nanopowders (after sintering).

3. Results and Discussion

X-ray diagrams of materials obtained by AM extrusion using a mixture of high-filled polymers (MEAM-HP) and Ti-Al intermetallide powders with subsequent sintering at 1100 ± 20 °C, 1200 ± 20 °C and 1250 ± 20 °C are shown in Figure 3a–c, respectively. The results of X-ray diffraction analysis are presented in Table 1.

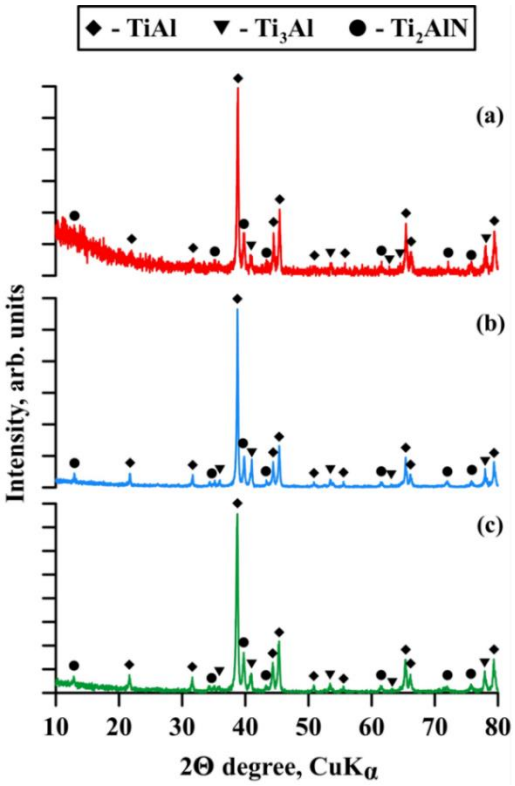

Figure 3. X-ray diagrams of the samples of additive-manufactured materials: sintering at 1100 °C (**a**); sintering at 1200 °C (**b**); sintering at 1250 °C (**c**).

Table 1. Results of X-ray diffraction analysis of materials obtained by AM extrusion from a mixture of high-filled polymers (MEAM-HP) and Ti-Al intermetallide powders with subsequent sintering.

Sintering Temperature, °C	Discovered Phases	Phase Content, wt%	Lattice Parameters, Å
1100	TiAl	82	a = 3.9900 c = 4.0715
	Ti_3Al	8	a = 5.7691 c = 4.6726
	Ti_2AlN	10	a = 3.0087 c = 13.6947
1200	TiAl	75	a = 4.0394 c = 4.0107
	Ti_3Al	12	a = 5.7699 c = 4.6814
	Ti_2AlN	13	a = 3.0184 c = 13.6517
1250	TiAl	74	a = 3.9911 c = 4.0728
	Ti_3Al	9	a = 5.8631 c = 4.6334
	Ti_2AlN	17	a = 3.0095 c = 13.6022

The phase composition of samples after sintering is represented by TiAl, Ti_3Al and Ti_2AlN phases. The lattice parameters of the phases obtained are comparable with the data obtained in [34–37], which suggests minimal distortion of their crystalline structure in the course of sintering. It is worth noting that the Ti_2AlN phase belongs to the MAX phases class; these classes possess a strong covalent bond, which leads to the emergence of a

unique combination of ceramic metal properties: improved rigidity, modulus of elasticity, heat conductivity, as well as resistance to wear, oxidation, thermal impact, superior resistance to mechanical damage, etc. [38–40]. Increases in the sintering temperature lead to changes in the concentration of phases in the samples. As the sintering temperature is raised from 1100 °C to 1200 °C, the ratio of the AlTi phase decreases from 82 to 75 wt%. Increasing the sintering temperature to 1250 °C does not incur a significant change in the weight ratio of this phase. Meanwhile, as the sintering temperature is raised from 1100 °C to 1200 °C, the ratio of the Ti_3Al phase increases from 8 to 12 wt%, and at the sintering temperature of 1250 °C, the ratio of the phase is reduced to 9 wt%. Additionally, increases in the sintering temperature lead to linear growth of the concentration of the Ti_2AlN MAX phase from 10 to 17 wt%. The research work [19] details the phase composition of Al-Ti intermetallides that were used in the present work. The authors have established that the composition of Al-Ti intermetallide powders is represented by Ti_3Al, TiAl and α-Ti phases that are in a solid solution with the content of aluminium up to 10 at% [41]. The authors of [34,41] report that α-Ti undergoes phase transition via two routes:

$$\alpha\text{-Ti} \longleftrightarrow Ti_3Al + TiAl \ (T = 1118.5\ ^\circ C), \quad (1)$$

$$\alpha\text{-Ti} \longleftrightarrow Ti_3Al \ (T = 1164\ ^\circ C), \quad (2)$$

Apart from that, works [42,43] report that Ti_3Al/TiAl phases interact with nitrogen (N_2), creating a Ti_2AlN MAX phase. From the research findings and literature data, we can make an assumption that phase transitions take place in the process of sintering of materials obtained by MEAM-HP. In the course of material sintering at 1100 ± 20 °C, diffusion processes are intensified, which leads to the transformation of α-Ti into Ti_3Al-TiAl. The obtained results and published data allow us to make an assumption about the existence of phase transformation during the sintering of materials obtained by the (MEAM-HP) method. During the sintering of materials at a temperature of 1100 ± 20 °C, diffusion processes intensify, which lead to the transformation of α-Ti into Ti_3Al-TiAl. It should be noted that the materials obtained in the process of sintering at a temperature of 1100 °C contain amorphous phases (2θ degree = 10–20°). In [44,45] reports the formation of amorphous phases of titanium nitride by thermochemical treatment of titanium-containing materials with ammonia at a temperature of 400–700 °C, as well as in the process of mechanical grinding of a mixture of titanium and hexagonal boron nitride. Literature data suggest that the amorphous phases of titanium nitride are formed during the annealing of samples from the polymer binder. The polymers contain polyimides, the main chain of which contains amide groups (−CONH−) [46]. During annealing at a temperature of 600 °C, nitrogen from amide groups interacts with intermetallic compounds, forming amorphous phases of titanium nitride. At a sintering temperature of 1100 °C, reactions of interaction of amorphous nitrides with Ti_3Al-TiAl intermettalides occur, which leads to the formation of the MAX-phase Ti_2AlN.

In addition, the transformation of α-Ti via route (1) leads to an increase in the weight ratio of TiAl in the sample compared to that of the initial powders and materials sintered at 1200 and 1250 °C. In the process of sample sintering at 1200 ± 20 °C, α-Ti transforms into Ti_3Al via route (2), which leads to an increase in the weight ratio of this phase in the sample. Apart from that, an increase in the sintering temperature leads to the intensification of the Ti_2AlN MAX phase creation processes and an increase in its concentration compared to samples sintered at 1100 ± 20 °C. The maximum concentration of the Ti_2AlN MAX phase is observed in the samples obtained at the sintering temperatures of 1250 ± 20 °C. In this case, the concentration of the Ti_3Al phase is decreased compared to materials obtained at the sintering temperature of 1200 ± 20 °C, and the concentration of the TiAl phase varies within the margin of measurement error (5–7%). It is assumed that at 1250 ± 20 °C, Ti_3Al reacts with nitrogen in the chamber more intensely compared to the TiAl phase, and this leads to a decrease in its concentration in the sintered samples. The works [47–49]

present the phase diagrams of the Al-Ti-N system at temperatures of 1000 and 1300 °C. The authors of the papers showed that the formation of the Ti_2AlN MAX phase at these temperatures occurs according to the mechanism of interaction between the Ti_3Al and TiN phases. Comparison of the obtained results with literature data shows that the mechanism of formation of the Ti_2AlN MAX phase at sample sintering temperatures, 1100, 1200 and 1250 °C, is comparable with the data presented on the phase diagrams of the Al-Ti-N ternary system at temperatures of 1000 and 1300 °C.

Figures 4–6 show structures of materials obtained by the MEAM-HP technique.

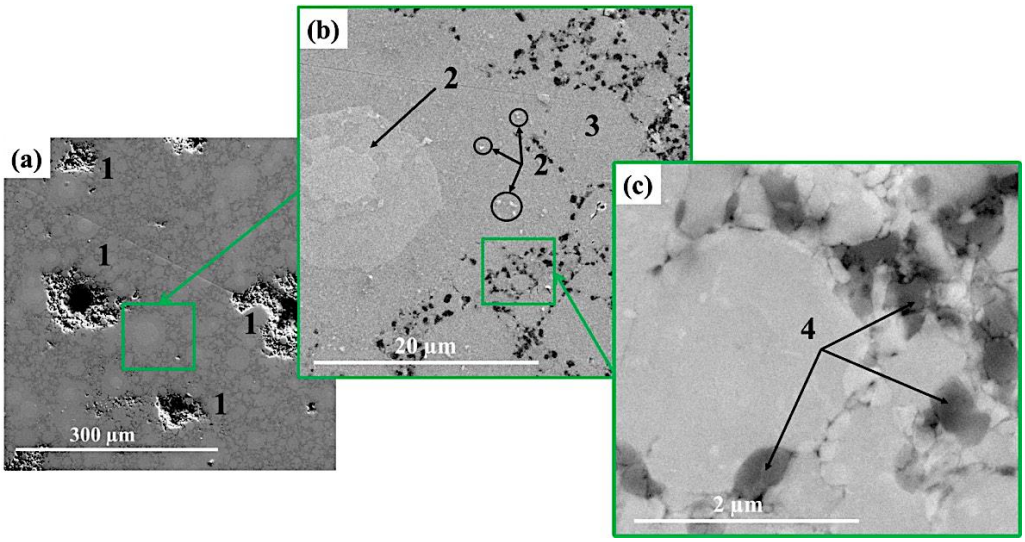

Figure 4. SEM image of materials obtained by MEAM-HP with subsequent sintering at 1100 ± 20 °C: ×550 (**a**), ×8300 (**b**), ×82 800 (**c**).

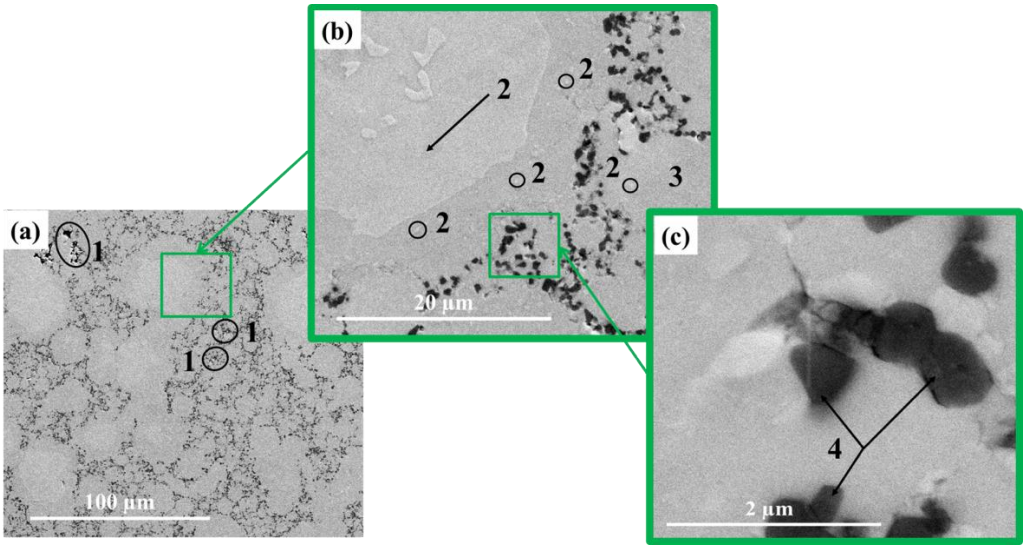

Figure 5. SEM image of materials obtained by MEAM-HP with subsequent sintering at 1200 ± 20 °C: ×1400 (**a**), ×8300 (**b**), × 82 800 (**c**)

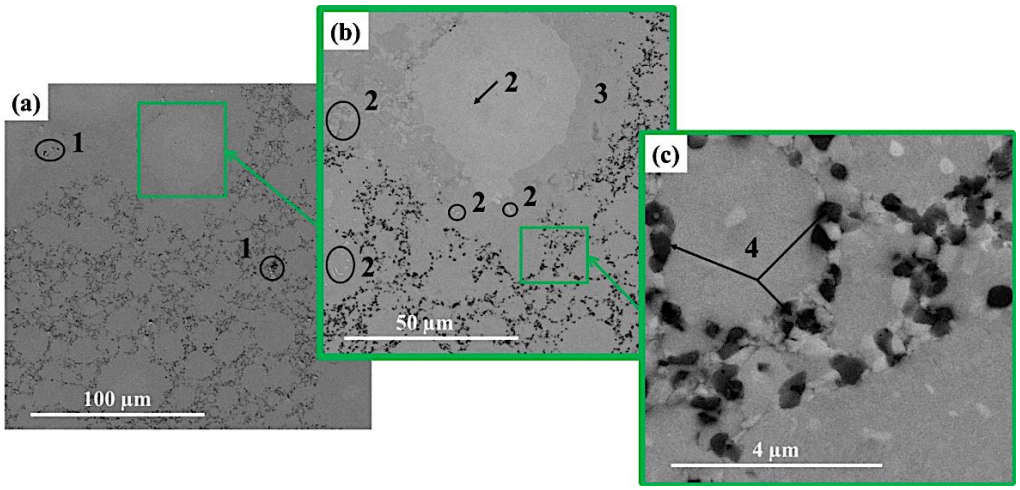

Figure 6. SEM image of the materials obtained by MEAM-HP with subsequent sintering at 1250 ± 20 °C: ×1400 (**a**),× 2800 (**b**) , × 41 400 (**c**)

Structures of materials obtained by sintering at different temperatures are represented by areas which have different contrast. In the matrix material of the Ti-Al intermetallide (area 3 in Figures 4b, 5b, 6b, respectively), large areas and particles of a lighter colour are observed (area 2 in Figures 4b, 5b, 6b, respectively) as well as black-coloured particles. Areas with different contrast are supposed to correspond to different phases present in the materials. In the structure of the materials obtained at the sintering temperature of 1100 ± 20 °C, isolated light-coloured areas and particles prevail, and do not exceed 30 μm in size. As the sintering temperature is raised to 1200 ± 20 °C and 1250 ± 20 °C, the size of light-coloured areas and particles increases to 50–60 μm and an isle structure is formed inside them. It is assumed that the growth of the size of areas and the formation of an isle structure is related to the processes of crystallite re-crystallisation in the phases present in the materials [50,51]. Figure 7b shows maps of chemical elements distribution. The results of energy-dispersive analysis of local areas of the materials structure are shown in Figure 6c and Table 2. Titanium and aluminium are the main elements present in the materials structure, and their concentration changes depending on the area in question. Nitrogen elements are concentrated in local areas (area 1 and 2) and in small particles; nitrogen corresponds to a lighter tint in the structures presented in Figures 3–5. By matching the obtained results against X-ray diffraction images and SEM images of the structures of the sintered materials, it was possible to determine the distribution of phases in the materials. It was found that the materials structure comprises an AlTi matrix with Ti_2AlN MAX-phase particles distributed within it and surrounded by a composite layer of Ti_3Al-Ti_2AlN. From the research findings, it was established that this layer is a transitional layer during the emergence of the Ti_2AlN MAX phase in the process of Ti_3Al intermetallide reaction with nitrogen. The research findings affirm the assumption that the Ti_3Al phase interacts more intensely with nitrogen compared to the TiAl phase, and it is the main source of the emergence of the Ti_2AlN MAX phase.

Elementary analysis of more contrasting particles (areas 7–8 in Figure 7a) present in the materials has shown the prevalence of elements of aluminium and oxygen, as well as the absence of elements of titanium and nitrogen. These particles are supposedly aluminium oxide. However, the aluminium oxide phase was not discovered by X-ray diffraction analysis, which is most probably due to its weak intensity compared to other phases, as well as its weight ratio below 5 wt%, which cannot be detected by XRD analysis techniques. It is assumed that Al_2O_3 particles emerged in the course of interaction of the aluminium component in α-Ti with titanium monoxide via aluminothermal reduction [52].

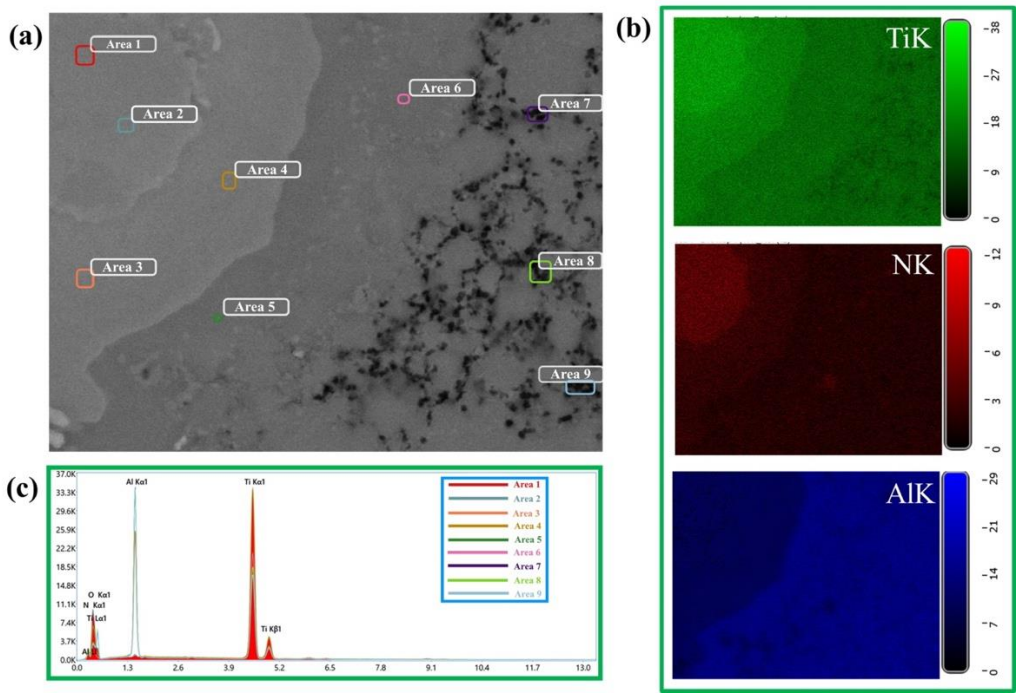

Figure 7. SEM image of the local materials area obtained by additive manufacturing via extrusion using a mixture of high-filled polymers (MEAM-HP) and Ti-Al intermetallide powders with subsequent sintering at 1100 ± 20 (**a**), maps of the distribution of chemical elements in a local area of a composite particle (**b**), results of the energy dispersive analysis of the local areas in the structure of the materials (**c**).

Table 2. Results of the energy-dispersive analysis of the local areas in the structure of the materials obtained by additive deposition from CrNi-TiN SHS composites using a mixture of high-filled polymers (MEAM-HP) and Ti-Al intermetallide powders with subsequent sintering at 1100 ± 20.

Area	Element, wt%			
	N_K	O_K	Al_K	Ti_K
1	8.4	<1	20.1	70.5
2	9.5	<1	19.9	69.6
3	4.3	<1	19.5	75.2
4	3.8	<1	18.8	76.4
5	1.5	<1	37.2	60.3
6	2.7	<1	36.4	59.9
7	<1	46.7	51.3	<1
8	<1	47.3	50.7	<1
9	<1	46.5	51.5	<1

Figure 8a shows an image of the distribution of hardness in material samples obtained via AM extrusion using a mixture of high-filled polymers (MEAM-HP) and Ti-Al intermetallide powders with subsequent sintering at 1100 ± 20 °C, 1200 ± 20 °C and 1250 ± 20 °C, respectively. It was found that materials sintered at 1100 ± 20 °C have close to linear hardness distribution, with rare minor deviations. Hardness varies in the range from 113 to 470 $HV_{0.1}$, and the average value is 193 $HV_{0.1}$. Increasing sintering temperature to 1200–1250 ± 20 °C leads to a significant distortion of hardness distribution in the samples obtained, which is represented by distinct peaks. The value of hardness is rapidly changing in the range between 115 and 1500 $HV_{0.1}$ (at the sintering temperature of 1200 ± 20 °C), and it reaches 1760 $HV_{0.1}$ (at the sintering temperature of 1250 ± 20 °C). Here, the

average microhardness of the samples increases from 193 to 690 $HV_{0.1}$ as the sintering temperature is raised from 1100 ± 20 °C to 1250 ± 20 °C (Figure 8b).

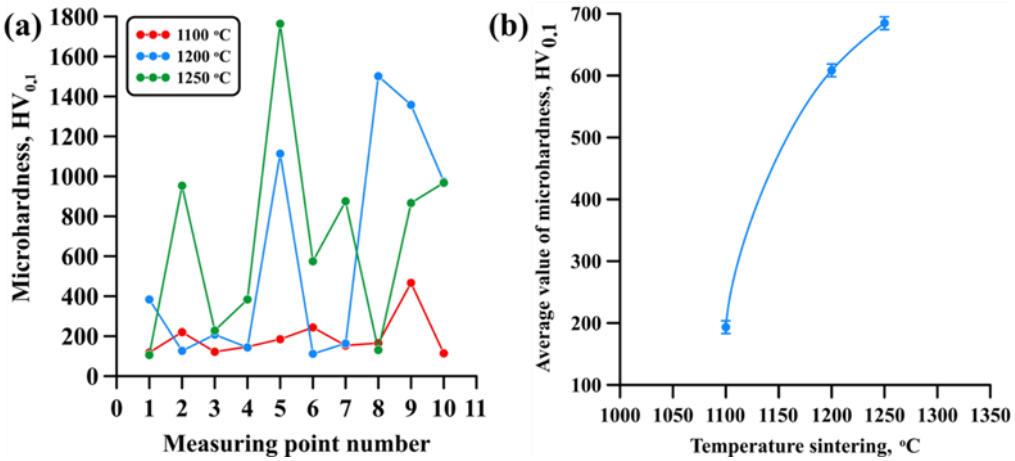

Figure 8. Graphical distribution of hardness in samples (**a**), dependency of sample hardness on the sintering temperature (**b**).

Changes in the nature of distribution of material hardness with increasing sintering temperature are related to an increase in the concentration and size of Ti_2AlN MAX phase particles, the hardness of that phase being as high as 4.1 GPa [53]. In the samples sintered at 1200-1250 ± 20 °C, MAX phase particles form agglomerates influenced by re-crystallisation processes and van der Waals forces, leading to the formation of an isle structure with large MAX phase areas [54,55]. When the indenter gets into this area, the recorded values vary between 1000 and 1760 $HV_{0.1}$, which results in the distortion of the distribution of hardness throughout the sample and peaks on the graphical representation. It was found by comparing the research findings with the results from [21,26] that the materials sintered at 1100 ± 20 °C have hardness comparable with the results from those works.

4. Conclusions

A schematic diagram of 3D printing using nanopowders of the ti-Al system is shown. This work researches the phase composition, structure and microhardness of materials obtained by AM extrusion using a mixture of high-filled polymers (MEAM-HP) and Ti-Al intermetallide powders with subsequent sintering at 1100 ± 20 °C, 1200 ± 20 °C and 1250 ± 20 °C. It was found that the materials structure comprises an AlTi matrix with Ti_2AlN MAX-phase particles distributed within it and surrounded by a composite layer of Ti_3Al-Ti_2AlN. Sintering temperature increases lead to changes in the concentration of TiAl, Ti_3Al and Ti_2AlN phases in the samples. Additionally, aluminium particles were discovered in the material structure; those emerged in the course of interaction of the aluminium component in α-Ti with titanium monoxide via an aluminothermal reduction mechanism. A mechanism explaining the formation of such a material structure was suggested, specifically; one for the particles of the Ti_2AlN MAX phase in the course of their sintering at different temperatures. It was found that the average microhardness of the samples increases from 193 to 690 $HV_{0.1}$ as the sintering temperature is raised from 1100 ± 20 °C to 1250 ± 20 °C.

Author Contributions: Conceptualisation, V.P. and M.L.; methodology, N.T. and A.B.; software, validation, N.S.; formal analysis, V.P.; investigation, V.P., A.B., A.M. and A.M.; writing—original draft preparation, V.P., A.M. and M.L.; writing—review and editing, N.S. and V.P.; visualisation, V.P.; supervision, A.V. and M.L. All authors have read and agreed to the published version of the manuscript.

Funding: This research was funded by the Russian Science Foundation, grant number 21-79-30006.

Data Availability Statement: Not applicable.

Conflicts of Interest: The authors declare no conflict of interest.

References

1. Williams, J.C.; Starke, E.A., Jr. Progress in structural materials for aerospace systems. *Acta Mater.* **2003**, *51*, 5775–5799.
2. Dimiduk, D.M. Gamma titanium aluminide alloys—An assessment within the competition of aerospace structural materials. *Mater. Sci. Eng. A* **1999**, *263*, 281–288.
3. Kaynak, Y.; Tascioglu, E. Finish machining-induced surface roughness, microhardness and XRD analysis of selective laser melted Inconel 718 alloy. *Procedia CIRP* **2018**, *71*, 500–504.
4. Brotzu, A.; Felli, F.; Marra, F.; Pilone, D.; Pulci, G. Mechanical properties of a TiAl-based alloy at room and high temperatures. *Mater. Sci. Technol.* **2018**, *34*, 1847–1853.
5. Clemens, H.; Mayer, S. Intermetallic titanium aluminides in aerospace applications–processing, microstructure and properties. *Mater. High Temp.* **2016**, *33*, 560–570.
6. Bewlay, B.P.; Nag, S.; Suzuki, A.; Weimer, M.J. TiAl alloys in commercial aircraft engines. *Mater. High Temp.* **2016**, *33*, 549–559.
7. Castellanos, S.D.; Cavalerio, A.J.; de Jesus, A.M.P.; Neto, R.; Lino Alves, J. Machinability of titanium aluminides: A review. *Proc. Inst. Mech. Eng. Part L J. Mater. Des. Appl.* **2019**, *233*, 426–451.
8. Loria, E.A. Quo vadis gamma titanium aluminide. *Intermetallics* **2001**, *9*, 997–1001.
9. Bünck, M.; Stoyanov, T.; Schievenbusch, J.; Michels, H.; Gußfeld, A. Titanium Aluminide Casting Technology Development. *JOM* **2017**, *69*, 2565–2570.
10. Wimler, D.; Lindemann, J.; Reith, M.; Kirchner, A.; Allen, M.; Vargas, W.G.; Franke, M.; Klöden, B.; Weißgärber, T.; Güther, V.; et al. Designing advanced intermetallic titanium aluminide alloys for additive manufacturing. *Intermetallics* **2021**, *131*, 107109.
11. Güther, V.; Allen, M.; Klose, J.; Clemens, H. Metallurgical processing of titanium aluminides on industrial scale. *Intermetallics* **2018**, *103*, 12–22.
12. Leyens, C.; Peters, M. *Titanium and Titanium Alloys: Fundamentals and Applications*, 1st ed.; WILEY-VCH Verlag Gmbh & Co. KGaA: Weinheim, Germany, 2003.
13. Zhao, L.; Wang, S.; Jin, Y.; Chen, Y. Microstructural characterization and mechanical performance of Al–Cu–Li alloy electron beam welded joint. *Aerosp. Sci. Technol.* **2018**, *82–83*, 61–69.
14. Şuta, S.; Thalmaier, G.; Sechel, N.; Vida-Simiti, I.; Petrescu, V. Ti-Al Membranes for Microfiltration. *Solid State Phenom.* **2016**, *254*, 8–13.
15. Böhm, A.; Kieback, B. Investigation of swelling behaviour of Ti–Al elemental powder mixtures during reaction sintering. *Int. J. Mater. Res.* **1998**, *89*, 90–95.
16. Yang, J.B.; Hwang, W.S. The preparation of TiAl-based intermetallics from elemental powders through a two-step pressureless sintering process. *J. Mater. Eng. Perform.* **1998**, *7*, 385–392.
17. Wang, G.X.; Dahms, M. An effective method for reducing porosity in the titanium aluminide alloy $Ti_{52}Al_{48}$ prepared by elemental powder metallurgy. *Scr. Metall. Mater.* **1992**, *26*, 1469–1474.
18. Dahms, M.; Schmelzer, F.; Seeger, J.; Wildhagen, B. Microstructure and mechanical properties of γ base titanium aluminide produced from extruded elemental powders. *Mater. Sci. Technol.* **1992**, *8*, 359–362.
19. Kennedy, S.; Kumaran, S.; Rao, T.S. Densification of γ-TiAl Powders by Spark Plasma Sintering. *Mater. Sci. Forum* **2012**, *710*, 303–307.
20. Mogale, N.F.; Matizamhuka, W.R. Spark Plasma Sintering of Titanium Aluminides: A Progress Review on Processing, Structure-Property Relations, Alloy Development and Challenges. *Metals* **2020**, *10*, 1080.
21. Park, K.; Kim, D.; Kim, K.; Cho, S.; Kwon, H. Behavior of Intermetallic Compounds of Al-Ti Composite Manufactured by Spark Plasma Sintering. *Materials* **2019**, *12*, 331.
22. Soliman, H.A.; Elbestawi, M. Titanium aluminides processing by additive manufacturing—A review. *Int. J. Adv. Manuf. Technol.* **2022**, *119*, 5583–5614.
23. Gibson, I.; Rosen, D.; Stucker, B.; Khorasani, M. *Additive Manufacturing Technologies*, 3rd ed.; Springer: Cham, Switzerland, 2021.
24. Wong, K.V.; Hernandez, A. A review of additive manufacturing. *Int. Sch. Res. Not.* **2012**, *2012*, 208760.
25. Khorasani, M.; Ghasemi, A.; Rolfe, B.; Gibson, I. Additive manufacturing a powerful tool for the aerospace industry. *Rapid Prototyp. J.* **2022**, *28*, 87–100.
26. Qu, H.P.; Li, P.; Zhang, S.Q.; Li, A.; Wang, H.M. The effects of heat treatment on the microstructure and mechanical property of laser melting deposition γ-TiAl intermetallic alloys. *Mater. Des.* **2010**, *31*, 2201–2210.
27. Chen, W.; Li, Z. 11—Additive manufacturing of titanium aluminides. In *Additive Manufacturing for the Aerospace Industry*; Elsevier: Amsterdam, The Netherlands, 2019; pp. 235–263.
28. Kim, Y.-W.; Dimiduk, D.M. Progress in the understanding of gamma titanium aluminides. *JOM* **1991**, *43*, 40–47.
29. Li, X.B.; Zhang, J.B.; Ji, X.C.; Wu, X.Q.; Luo, J.S.; Tang, Y.J. A Small Patch Production of γ-TiAl Alloys Nanoparticles via Physical Vapor-phase Method. *Integr. Ferroelectr.* **2013**, *147*, 146–153.

30. Lerner, M.; Pervikov, A.; Glazkova, E.; Rodkevich, N.; Toropkov, N. Electrical Explosion Synthesis, Oxidation and Sintering Behavior of Ti-Al Intermetallide Powders. *Metals* **2021**, *11*, 760.
31. Jones, S.A.; Kaufman, M.J. Phase equlibria and transformations in intermediate titanium-aluminum alloys. *Acta Metall. Mater.* **1993**, *41*, 387–398.
32. Gonzalez-Gutierrez, J.; Cano, S.; Schuschnigg, S.; Kukla, C.; Sapkota, J.; Holzer, C. Additive Manufacturing of Metallic and Ceramic Components by the Material Extrusion of Highly-Filled Polymers: A Review and Future Perspectives. *Materials* **2018**, *11*, 840.
33. Seyedzavvar, M.; Boğa, C. A study on the effects of internal architecture on the mechanical properties and mixed-mode fracture behavior of 3D printed $CaCO_3$/ABS nanocomposite samples. *Rapid Prototyp. J.* **2022**. https://doi.org/10.1108/RPJ-09-2021-0244
34. Batalu, D.; Cosmeleata, G.; Aloman, A. Critical analysis of the Ti-Al phase diagrams. *UPB Sci. Bull. Ser. B Chem. Mater. Sci.* **2006**, *68*, 77–90.
35. Villars, P.; Calvert, L.D. *Pearson's Handbook of Crystallographic Data for Intermediate Phases*; American Society of Metals: Cleveland, OH, USA, 1985.
36. Manoun, B.; Zhang, F.X.; Saxena, S.K.; El-Raghy, T.; Barsoum, M.W. X-ray high-pressure study of Ti_2AlN and Ti_2AlC. *J. Phys. Chem. Solids* **2006**, *67*, 2091–2094.
37. Hug, G.; Jaouen, M.; Barsoum, M.W. X-ray absorption spectroscopy, EELS, and full-potential augmented plane wave study of the electronic structure of Ti_2AlC, Ti_2AlN, Nb_2AlC, and $(Ti_{0.5}Nb_{0.5})_2AlC$. *Phys. Rev. B.* **2005**, *71*, 024105.
38. Barsoum, M.W. The MN+ 1AXN phases: A new class of solids: Thermodynamically stable nanolaminates. *Prog. Solid State Chem.* **2000**, *28*, 201–281.
39. Barsoum, M.W. *MAX Phases: Properties of Machinable Ternary Carbides and Nitrides*, 1st ed.; WILEY-VCH Verlag Gmbh & Co. KGaA: Weinheim, Germany, 2013.
40. Hanaor, D.; Hu, L.; Kan, W.H.; Proust, G.; Foley, M.; Karaman, I.; Radovic, M. Compressive performance and crack propagation in Al alloy/Ti2AlC composites. *Mater. Sci. Eng. A* **2016**, *672*, 247–256.
41. Kattner, U.R.; Lin, J.-.-C.; Chang, Y.A. Thermodynamic Assessment and Calculation of the Ti-Al System. *Met. Mater. Trans. A* **1992**, *23*, 2081–2090.
42. Chlubny, L.; Lis, J.; Buko, M.M. Influence of nitrogen pressure on shs synthesis of Ti_2AlN Powders. In *Proceedings of the Developments in Strategic Ceramic Materials: A Collection of Papers Presented at the 39th International Conference on Advanced Ceramics and Composites*, 1st ed.; Kriven, W.M., Wang, J., Zhu, D., Fisher, T., Eds.; John Wiley & Sons: Hoboken, NJ, USA, 2016; p. 253.
43. Tian, J.J.; Zhang, L.L.; Bi, X.W.; Liu, G.Y.; Ding, Z.M. Ti_2AlN Prepared by Self-Propagating High-Temperature Combustion Method Using TiN as Additive. *Adv. Mater. Res.* **2013**, *710*, 37–40.
44. Bailey, E.; Ray, N.; Hector, A.L.; Crozier, P.; Petuskey, W.T.; McMillan, P.F. Mechanical properties of titanium nitride nanocomposites produced by chemical precursor synthesis followed by high-P,T treatment. *Materials* **2011**, *4*, 1747–1762.
45. Ding, Z.H.; Yao, B.; Qiu, L.X.; Bai, S.Z.; Guo, X.Y.; Xue, Y.F.; Wang, W.R.; Zhou, X.D.; Su, W.H. Formation of titanium nitride by me-chanical milling and isothermal annealing of titanium and boron nitride. *J. Alloys Compd.* **2005**, *391*, 77–81.
46. Deopura, B.L.; Alagirusamy, R.; Joshi, M.; Gupta, B. *Polyesters and Polyamides,* 1st ed.; Woodhead Publishing Limited: Cambridge, UK, 2008.
47. Procopio, A.; El-Raghy, T.; Barsoum, M. Synthesis of Ti 4 AlN 3 and phase equilibria in the Ti-Al-N system. *Metall. Mater. Trans. A* **2000**, *31*, 373–378.
48. Chen, Q.; Sundman, B. Thermodynamic assessment of the Ti-Al-N system. *J. Phase Equilibria Diffus.* **1998**, *19*, 146–160.
49. Magnan, J.; Weatherly, G.C.; Cheynet, M.-.-C. The nitriding behavior of Ti-Al alloys at 1000 °C. *Met. Mater. Trans. A* **1999**, *30*, 19–29.
50. Huang, K.; Marthinsen, K.; Zhao, Q.; Logé, R.E. The double-edge effect of second-phase particles on the recrystallization behaviour and associated mechanical properties of metallic materials. *Prog. Mater. Sci.* **2018**, *92*, 284–359.
51. Sadovnikov, S.I.; Gusev, A.I. The Effect of Temperature on the Particle Sizes and the Recrystallization of Silver Sulfide Nanopowders. *Phys. Solid State* **2018**, *60*, 1308–1315.
52. Osinkina, T.V.; Krasikov, S.A.; Zhilina, E.M.; Agafonov, S.N.; Vedmid', L.B.; Zhidovina, S.V. Influence of niobium and tantalum on the phase formation during the metallothermic interaction of aluminum with titanium dioxide. *Russ. Metall. (Met.)* **2019**, *2019*, 85–89.
53. Lin, Z.; Zhuo, M.; Li, M.; Wang, J.; Zhou, Y. Synthesis and microstructure of layered-ternary Ti_2AlN ceramic. *Scr. Mater.* **2007**, *56*, 1115–1118.
54. Seipenbusch, M.; Rothenbacher, S.; Kirchhoff, M.; Schmid, H.-J.; Kasper, G.; Weber, A.P. Interparticle forces in silica nanoparticle agglomerates. *J. Nanopart. Res.* **2010**, *12*, 2037–2044.
55. Xuan, C.; Karasev, A.V.; Jönsson, P.G.; Nakajima, K. Attraction force estimations of Al_2O_3 particle agglomerations in the melt. *Steel Res. Int.* **2017**, *88*, 1600090.